where γ is the collection of all sites connected to X through drainage directions. The theorem predicts that, for efficient drainage basins, a log–log plot of C versus A should have a slope of 3/2 because $D = 2$ and river networks in nature are known to be efficient and directed[12]. Our observational data (Fig. 2) are found to agree with the predictions over five decades of scales.

Our general results should be applicable to a wide variety of distributed networks including the flow of water, blood, sewage, food, air and electrical currents. Even though the specific details vary significantly, the novel behaviour built into efficient transportation networks provides a unified framework[13] underlying the allometric scaling of diverse systems. □

Received 17 August 1998; accepted 10 March 1999.

1. McMahon, T. A. & Bonner, J. T. *On Size and Life* (Scientific American Library, New York, 1983).
2. Bonner, J. T. *The Evolution of Complexity by Means of Natural Selection* (Princeton Univ. Press, Princeton, 1983).
3. Peters, R. H. *The Ecological Implications of Body Size* (Cambridge Univ. Press, Cambridge, 1983).
4. Feldman, H. A. & McMahon, T. A. The 3/4 mass exponent for energy metabolism is not an artifact. *Respir. Physiol.* **52,** 149–163 (1983).
5. Schmidt, Nielsen, K. *Scaling: Why is Animal Size so Important?* (Cambridge Univ. Press, Cambridge, 1984).
6. Calder, W. A. III *Size, Function and Life History* (Harvard Univ. Press, Cambridge, Massachusetts, 1984).
7. Brown, J. H. *Macroecology* (Univ. Chicago Press, Chicago, 1995).
8. West, G. B., Brown, J. H. & Enquist, B. J. A general model for the origin of allometric scaling laws in biology. *Science* **276,** 122–126 (1997).
9. Enquist, B. J., Brown, J. H. & West, G. B. Allometric scaling of plant energetics and population density. *Nature* **395,** 163–165 (1998).
10. Damuth, J. D. Common rules for animals and plants. *Nature* **395,** 115–116 (1998).
11. Stevens, P. S. *Patterns in Nature* (Little, Brown, Boston, 1974).
12. Rodriguez-Iturbe, I. & Rinaldo, A. *Fractal River Basins: Chance and Self-Organization* (Cambridge Univ. Press, New York, 1997).
13. Wilson, E. O. *Consilience: The Unity of Knowledge* (Knopf, New York, 1997).

Supplementary information is available on *Nature*'s World-Wide Web site (http://www.nature.com) or as paper copy from the London editorial office of *Nature*.

Acknowledgements. We thank R. Rigon for the computations shown in Fig. 2; A. Beauvais, F. Colaiori, P. Dodds, A. Flammini, M. Caterina Putti, R. Robinett, I. Rodriguez-Iturbe, D. Rothman and J. Weitz for helpful discussions; and John Damuth for many key insights. This work was supported by INFN, NASA, NATO, MURST 40% *Trasporto di sedimenti ed evoluzione morfologica di corsi d'acqua, estuari e lagune alle diverse scale temporali* and The Donors of the Petroleum Research Fund administered by the American Chemical Society.

Correspondence and requests for materials should be addressed to J.R.B. (e-mail: jayanth@phys.psu.edu).

Electronic mechanism of hardness enhancement in transition-metal carbonitrides

Seung-Hoon Jhi*, Jisoon Ihm*, Steven G. Louie† & Marvin L. Cohen†

** Department of Physics and Center for Theoretical Physics, Seoul National University, Seoul 151-742, Korea*
† Department of Physics, University of California at Berkeley, Berkeley, California 94720–7300, USA
and Materials Science Division, Lawrence Berkeley National Laboratory, Berkeley, California 94720, USA

Transition-metal carbides and nitrides are hard materials widely used for cutting tools and wear-resistant coatings. Their hardness is not yet understood at a fundamental level. A clue may lie in the puzzling fact that transition-metal carbonitrides that have the rock-salt structure (such as TiC_xN_{1-x}) have the greatest hardness for a valence-electron concentration of about 8.4 per cell[1–3], which suggests that the hardness may be determined more by the nature of the bonding than by the conventional microstructural features that determine the hardness of structural metals and alloys. To investigate this possibility, we have evaluated the shear modulus of various transition-metal carbides and nitrides using *ab initio* pseudopotential calculations. Our results show that the behaviour of these materials can be understood on a fundamental level in terms of their electronic band structure. The unusual hardness originates from a particular band of σ bonding states between the non-metal *p* orbitals and the metal *d* orbitals that strongly resists shearing strain or shape change. Filling of these states is completed at a valence-electron concentration of about 8.4, and any additional electrons would go into a higher band which is unstable against shear deformations.

Among the various microscopic and intrinsic properties of materials, the shear modulus provides a measure of the rigidity against the shape deformations involved in microhardness indentation experiments. In particular, since the Peierls stresses in the transition-metal carbonitrides are very high, the strengths of these compounds may be influenced more by the difficulty of nucleating and moving dislocations through the background crystal lattice than by the difficulty of moving dislocations through microstructural obstacles[4]. As the stresses required to nucleate or move isolated dislocations scale with the shear modulus, electronic changes that affect the shear modulus may have a pronounced effect on the macroscopic hardness value. Several prior discussions of the mechanical properties of hard materials have made this point[4–8]. There is more than one shear modulus, but we have elected to study c_{44} (rather than, say, the difference between c_{11} and c_{12} or averaged shear modulus) which by itself represents a shape change without volume change, and provides directly information about electronic response to shear strain.

To understand the variation of the shear modulus c_{44} with composition, we carried out quantum-mechanical electronic-structure calculations (under both normal and strained conditions) for TiC_xN_{1-x}, HfC_xN_{1-x} and $Zr_xNb_{1-x}C$ using the *ab initio* pseudopotential method[9,10]. In our calculations, alloy configurations such as TiC_xN_{1-x} are simulated in two different ways and cross-checked. The first is the virtual crystal method in which the ionic pseudopotential

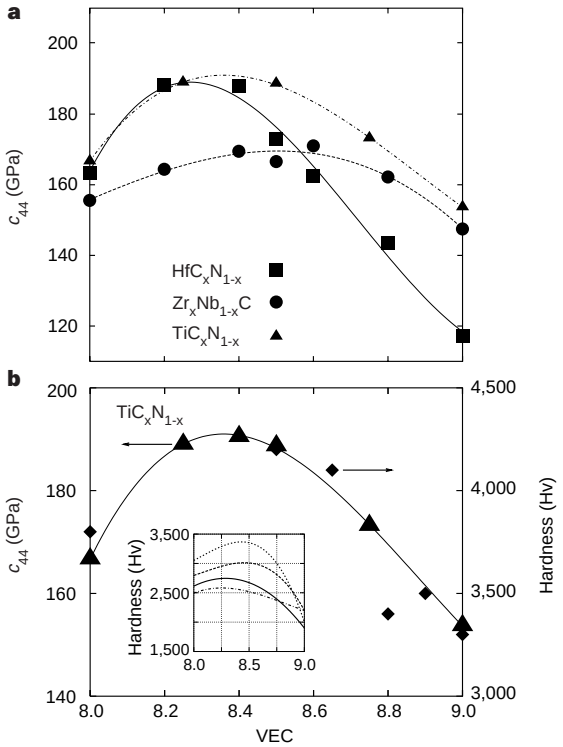

Figure 1 Correlation between the calculated shear modulus c_{44} and experimental microhardness. **a**, Calculated shear modulus c_{44} in GPa for TiC_xN_{1-x} (filled triangles), HfC_xN_{1-x} (filled boxes) and $Zr_xNb_{1-x}C$ (filled circles) as a function of the valence electron concentration (VEC). The curves are polynomial fits to the calculated c_{44}. **b**, Measured microhardness of TiC_xN_{1-x} cermets from ref. 2 in Hv units (filled diamonds). For comparison, the calculated c_{44} (filled triangles) in GPa is plotted in the same figure. The thin solid line is a guide to the eye. Inset, microhardness of bulk alloys and sub-stoichiometric compounds (Ti(CN), dotted line; (ZrNb)C, dashed line; Hf(CN), solid line; and NbC_{1-x}, dash-dotted line).

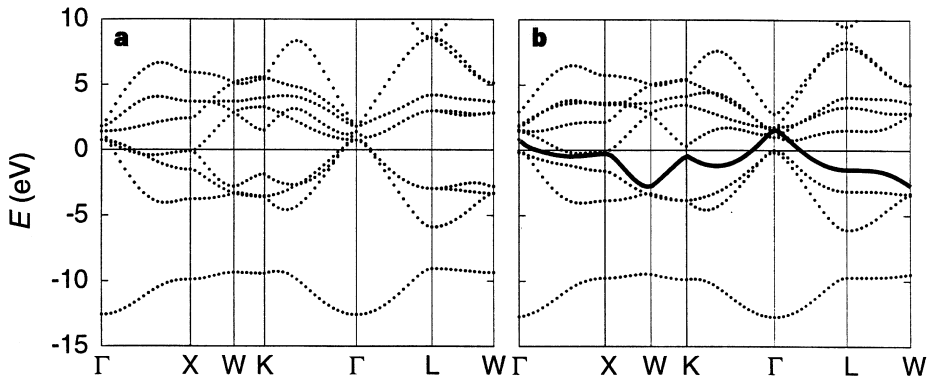

Figure 2 Influence of shear strain on the electronic structure of TiC. **a**, Electronic band structure at zero strain. **b**, Electronic band structure at finite shear strain ($\epsilon_{xy} = 0.1$). For comparison, the band structure of sheared TiC is plotted along the symmetry line equivalent to that of the face-centred cubic (f.c.c.) structure. The Fermi level lies at the energy zero. If carbon atoms are replaced by nitrogen atoms in TiC_xN_{1-x} alloys, extra electrons from nitrogen will occupy the empty states just above the Fermi level at first, and then fill higher-lying metallic conduction bands as the nitrogen concentration increases further. The fourth band shows a larger rise in energy on the application of the shear stress (solid line in **b**) compared with its unstrained counterpart in **a**. The fifth band in **b**, by contrast, is lowered in energy compared with that in **a**.

for, say, C_xN_{1-x} is approximated by the weighted average of those of C and N and then the usual *ab initio* self-consistent pseudopotential calculation is done. The second is a supercell method, with a set of particular atomic arrangements chosen to mimic random alloys. No assumption is made about the electronic structure, and a fully self-consistent calculation is performed. The two methods yield results within a few per cent of each other and the trend found is identical.

Figure 1a shows the calculated shear modulus as a function of the valence-electron concentration (VEC). For all cases shown (TiC_xN_{1-x}, $Zr_xNb_{1-x}C$ and HfC_xN_{1-x}), $x = 1$ corresponds to a VEC of 8 (electrons per unit cell) and $x = 0$ to a VEC of 9. The shear modulus c_{44} shows a maximum value for VEC in the range 8.3–8.5. In Fig. 1b, we show together the experimental microhardness (in Vickers hardness scale, Hv) and the calculated c_{44} of TiC_xN_{1-x} to demonstrate the close correlation between the two. Experimental hardnesses for other materials are plotted in the inset to show that the trends are essentially the same. To understand in more detail the behaviour of c_{44} common to all these materials, we choose TiC_xN_{1-x} as a representative material and discuss the change in its electronic structure under shear strain.

Figure 2 shows the band structure of TiC at equilibrium and under the shear strain of $\epsilon_{xy} = \epsilon_{yx} = 0.1$. Three states derived from carbon $2p$ orbitals, degenerate at the Γ-point, split into two inequivalent states of $p_x + p_y$ and p_z symmetry under the shear strain. The metal d orbitals of e_g symmetry also split into $d_{3z^2-r^2}$ and $d_{x^2-y^2}$ states in the second and fourth band, respectively, of the strained electronic band structure. As seen in the figure, drastic change occurs along the symmetry line K–Γ–L near the Fermi level: we note the conspicuous rise of the fourth band relative to other bands, under the shear strain. The movement of the fourth band is closely related to its highly directional bonding character (Fig. 3a). In the region near K, the fourth band is mainly derived from σ bonding interactions between the titanium $d_{x^2-y^2}$ orbitals and the carbon p_x and p_y orbitals. Optimal bonding occurs when the Ti–C–Ti bond angle is 90°. Under the shear strain, this angle deviates from the optimal geometry and the energy level of the fourth band rises to second order in ϵ_{xy}. The large increase in the electronic energy under shear strain shows that electrons occupying the fourth band are extremely resistive to shear. The second and third bands mainly consist of π bonding between p and d orbitals which is relatively insensitive to the shear distortion. But the metallic σ bonding states in the fifth band, derived from d–d interactions, are very sensitive to the shear strain. Due to the strengthening of the metal–metal bonding along the $[1\bar{1}0]$ direction by the shortening of the inter-metallic distance under shear strain (Fig. 3b), this band is lowered giving rise to a negative contribution to the elastic shear modulus if it is occupied. Along the Γ–L line, a similar analysis holds, but the bonding character is complicated by the influence of the third-nearest-neighbour atoms.

The strain energy density for a symmetric shear strain $e_{xy} = \epsilon_{xy} + \epsilon_{yx}$ is given by:

$$u(e_{xy}) = \frac{1}{2} c_{44} e_{xy}^2 \qquad (1)$$

As the energy rise of the fourth band is second order in the shear strain ϵ_{xy}, electrons occupying this band contribute positively to the shear modulus. As x decreases from 1 in the TiC_xN_{1-x} alloys, additional electrons provided by the nitrogen atoms occupy the empty states of the fourth band near the Γ-point (degenerate with the second and third bands in the absence of the strain) and enhance c_{44}. At $x \approx 0.6$, corresponding to VEC = 8.4, the Fermi level lies at the local valence band maximum at the Γ-point and the fourth band is completely filled. When the carbon concentration (expressed as x)

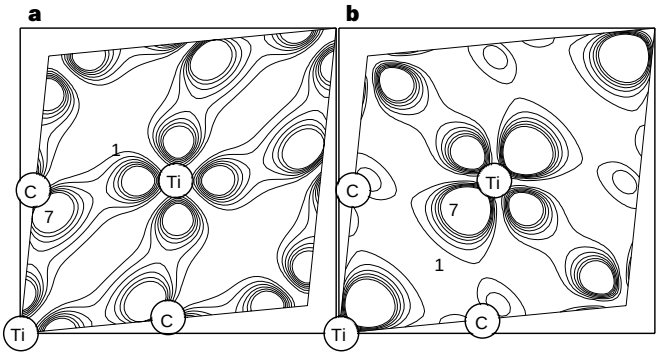

Figure 3 Charge density of a state of TiC near the K-point of the Brillouin zone under shear strain ($\epsilon_{xy} = 0.1$). **a**, Charge-density plot of the fourth band on the (001) plane. **b**, Charge-density plot of the fifth band on the same plane as in **a**. When shear strain is absent, the bonding character of the fourth band is covalent $pd\sigma$ bonding between titanium (Ti) and carbon (C), and that of the fifth band is weak $dd\sigma$ metallic bonding. The contour line step is 1 electron per unit cell, and the charge density increases from zero (in the interstitial region) to 7 electrons per unit cell (around atomic sites). As the shear strain distorts the bond axis of the $pd\sigma$ bonding in the fourth band and raises the energy level, electrons occupying the fourth band give a positive contribution to the elastic shear modulus. On the other hand, electrons in the fifth band give a negative contribution to the shear modulus because the shear strain enhances the bond strength of metallic $dd\sigma$ bonding and lowers the energy level.

decreases well below 0.6, a local gap opens at the Γ-point and the band structure looks similar to that of TiN. The decrease of c_{44} at $x \leq 0.6$ is attributed in large part to the filling of the fifth band near the K-point which gives a large negative contribution to c_{44} as mentioned above. Hence the occurrence of the shear-modulus maximum at the VEC of ~8.4 originates from the complete filling of the shear-resistive $pd\sigma$ bonding states at this electron concentration. The occurrence of the experimental microhardness maximum at the same VEC strongly suggests the same origin for the hardness (see below).

Generally speaking, hardness is determined by the mobility of dislocations. A central question is then whether the creation and motion of dislocations in our materials can be correlated with a simpler and more fundamental property, such as the shear modulus. For the covalently bonded materials, the very low mobility of dislocation kinks is the rate-determining factor for dislocation motion and is in turn determined by the very high bond-breaking energy under a large shear strain. The bond-breaking energy involved in plastic deformation and the bond-restoring energy under elastic shear strain essentially go together in covalently bonded hard materials. This reasoning indicates that the response of well-localized bonds (such as covalent bonds) to shear is the crucial factor in determining hardness. For many $s-p$ tetrahedrally bonded semiconductors, their hardness also shows a strong correlation with the bulk modulus, which has been a focus of some previous theoretical work[11]. The shear modulus, however, encompasses a greater set of materials as a general indicator of hardness.

The microhardness of the alloys considered here is about 17–23 GPa, approximately one-eighth of the calculated c_{44}. In indentation tests, materials deform typically with about 8–12% strain, on average[2], and the hardness is of the same magnitude as the yield stress. The ratio of the hardness to the calculated c_{44} indicates that the yield stress or the critical shear stress of the alloys is close to the theoretical value of the perfect crystals ($1/2\pi$ times the shear modulus), which is a common feature of covalently bonded materials[13]. The highly directional coupling between metal d and non-metal $2p$ electrons results in a shear-resistive covalent bonding in the present case. The kink migration energy is typically a few tenths of the cohesive energy for covalently bonded materials (for bulk silicon, it is[14] ~1.6 eV, about one-third of the experimental cohesive energy of 4.63 eV), exceeding the typical strain energy in indentation tests. Under such circumstances, dislocations are hard to activate at low temperature, and the critical shear stress is expected to be close to that of the perfect crystal. In short, in the plastic deformation of these materials, slip occurs in a manner expected of a perfect crystal, and the shear modulus is a good measure to quantify the resistance to plastic deformation.

Using this argument, other transition-metal alloys with the rock-salt structure are expected to have maximum hardness at the same VEC (~8.4). In fact, it has been experimentally verified[1] that $Ti_xNb_{1-x}C$ has a hardness trend similar to that of $Zr_xNb_{1-x}C$. Moreover, our theory may be used to explain the hardness behaviour of the sub-stoichiometric group V carbides. The hardness of such carbides is found[1,3] to have a maximal value at a specific vacancy concentration of ~12%. If the electronic structures of sub-stoichiometric compounds are not much changed from those of the stoichiometric phase, the maximal hardness is expected at the vacancy concentration which gives a VEC of 8.4; that is, 12.5%, in agreement with the above observation. However, one should be cautious about generalizing this argument, as a significant deviation from stoichiometry may alter the shape and character of the band structure. In addition, the behaviour of the hardness (and correspondingly, the elastic shear modulus) of sub-stoichiometric transition-metal compounds may depend on the microstructure of the vacancies; for example, aggregates of vacancies[15] may occur. Some sub-stoichiometric nitrides indeed show different hardness trends with varying vacancy concentrations[1,16].

We note that the bulk modulus of metallic hard materials does not show a maximum between VEC values of 8 and 9. The anomalous maximum in hardness or c_{44} of these materials is attributed to the presence near the Fermi level of two electronic bands that respond oppositely to shear stress. Under hydrostatic pressure, on the other hand, symmetry is preserved and all bands are resistive to volume change. The bulk modulus has been shown theoretically[17] to be a monotonic function of the VEC. The presence of bands of two different bonding characters near the Fermi level makes the hard transition-metal alloys distinct from semiconductors or insulators where the bulk modulus, shear modulus, and hardness all show the same trends. □

Received 11 December 1998; accepted 22 March 1999.

1. Holleck, M. Material selection for hard coatings. *J. Vac. Sci. Technol. A* **4,** 2661–2669 (1986).
2. Richter, V., Beger, A., Drobniewski, J., Endler, I. & Wolf, E. Characterization and wear behavior of TiN- and TiC_xN_{1-x}-coated cermets. *Mater. Sci. Eng. A* **209,** 353–357 (1996).
3. Toth, L. E. *Transition Metal Carbides and Nitrides* (Academic, New York, 1971).
4. Kelly, A. & Macmillan, N. H. *Strong Solids* 3rd edn (Clarendon, Oxford, 1986).
5. Gilman, J. J. The plastic resistance of crystals. *Aust. J. Phys.* **13,** 327–346 (1960).
6. Clerc, D. G. & Ledbetter, H. M. Mechanical hardness: a semiempirical theory based on screened electrostatics and elastic shear. *J. Phys. Chem. Solids* **59,** 1071–1095 (1998).
7. Teter, D. M. Computational alchemy: the search for new superhard materials. *Mater. Res. Soc. Bull.* **23,** 22–27 (1998).
8. Krenn, C. R., Morris, J. W., Jhi, S.-H. & Ihm, J. in *Hard Coatings Based on Borides, Carbides & Nitrides* (eds Kumar, A., Chung, Y.-W. & Chia, R. W. J.) 379–388 (The Minerals, Metals & Materials Soc., Warrendale, PA, 1998).
9. Ihm, J., Zunger, A. & Cohen, M. L. Momentum-space formalism for the total energy of solids. *J. Phys. C* **12,** 4409–4422 (1979).
10. Pickett, W. E. Pseudopotential methods in condensed matter applications. *Comput. Phys. Rep.* **9,** 115–197 (1989).
11. Liu, A. Y. & Cohen, M. L. Prediction on new low compressibility solids. *Science* **245,** 841–842 (1989).
12. Samuels, L. E. in *Microindentation Technique in Materials Science and Engineering* (eds Blau, P. J. & Lawn, B. R.) 5–24 (ASTM, Philadelphia, 1985).
13. Gilman, J. J. Physical chemistry of intrinsic hardness. *Mater. Sci. Eng. A* **209,** 74–81 (1996).
14. Nikitenko, V., Farber, B. & Iunin, Yu. Experimental investigation of the dynamics of kinks of dislocation lines in semiconductor single crystals. *Sov. Phys. JETP* **66,** 738–746 (1987).
15. Hull, D. & Bacon, D. J. *Introduction to Dislocations* 3rd edn (Pergamon, Oxford, 1984).
16. Jiang, X. *et al.* Elastic constants and hardness of ion-beam-sputtered TiN_x films measured by Brillouin scattering and depth-sensing indentation. *J. Appl. Phys.* **69,** 3053–3057 (1991).
17. Jhi, S.-H. & Ihm, J. Electronic structure and structural stability of TiC_xN_{1-x} alloys. *Phys. Rev. B* **56,** 13826–13829 (1997).

Acknowledgements. S.-H.J. and J.I. were supported by the SNI, the SRC programme of KOSEF, and the BSRI programme of KRF. S.G.L. and M.L.C. were supported by the NSF and DOE. The support of a Korea-US Cooperative Grant by KOSEF and NSF is acknowledged. S.G.L acknowledges the hospitality of the Korea Institute for Advanced Study, where part of this Letter was written.

Correspondence and requests for materials should be addressed to S.G.L. (e-mail: louie@uclink4.berkeley.edu).

Near-field probing of vibrational absorption for chemical microscopy

B. Knoll & F. Keilmann

Max-Planck-Institut für Biochemie, D-82152 Martinsried, Germany

Identification of chemical compounds by vibrational spectroscopy at infrared wavelengths requires macroscopic samples: the spatial resolution is diffraction-limited to a scale of about half the wavelength, or about five micrometres. The scanning near-field optical microscope[1,2], however, can reveal sub-wavelength detail because it uses near-field probing rather than beam focusing. Here we demonstrate the use of the aperture-less approach to scanning near-field optical microscopy[3–6] to obtain contrast in vibrational absorption on a scale of about 100 nanometres, about one-hundredth of a wavelength. We record infrared scattering from the tip of an atomic force microscope scanned over a composite polymer film. At the boundary between different polymers we observe contrast changes owing to changes in vibrational absorption. The contrast is strongly enhanced in the near field of the probe tip, which we interpret as evidence of surface-enhanced infrared absorption[7]. When extended to multi-wavelength opera-